Check for updates

Clinical & Experimental Ophthalmology

WILEY

Clinical & Experimental Ophthalmology

ORIGINAL ARTICLE-CLINICAL SCIENCE OPEN ACCESS

Correcting Axial Length-Related Magnification Errors in Optical Coherence Tomography Angiography Improves Machine Learning Classification Performance in High Myopia

Danuta M. Sampson[1] | Mila Yue Zhang[1] | Hemn Baghban Jaldian[2] | Madeleine S. Torcasso[3] | Gavrielle R. Untracht[4] | Jocelyn J. Drinkwater[1,5] | Mei Zhao[6] | David D. Sampson[7] | Andrew Lam[6] | Fred K. Chen[1,8,9]

[1]Centre for Ophthalmology and Visual Science (Incorporating Lions Eye Institute), The University of Western Australia, Perth, Australia | [2]Department of Optometry, School of Rehabilitation, Shahid Beheshti University of Medical Sciences, Tehran, Iran | [3]Department of Medicine, University of Chicago, Chicago, Illinois, USA | [4]Department of Health Technology, Technical University of Denmark, Kongens Lyngby, Denmark | [5]Lions Outback Vision, Nedlands, Australia | [6]Centre for Myopia Research, School of Optometry, Faculty of Health and Social Science, The Hong Kong Polytechnic University, Kowloon, Hong Kong, China | [7]School of Computer Science and Electronic Engineering, The University of Surrey, Guildford, UK | [8]Department of Ophthalmology, Royal Perth Hospital, Perth, Australia | [9]Ophthalmology, Department of Surgery, University of Melbourne, Melbourne, Australia

Correspondence: Danuta M. Sampson (danuta.sampson@uwa.edu.au) | Fred K. Chen (fred.chen@lei.org.au)

Received: 29 January 2026 | **Revised:** 12 August 2026 | **Accepted:** 24 August 2026

Keywords: classification task | myopia | optical coherence tomography angiography | retina | retinal magnification factor

ABSTRACT

Background: To determine whether axial length-related magnification correction in optical coherence tomography angiography (OCTA) improves machine learning classification of high myopia and resolves inconsistencies in the values and discriminatory power of OCTA microvascular metrics.

Methods: We analysed retinal OCTA images from a prior Hong Kong Polytechnic University study. Fourteen superficial vascular plexus metrics were extracted before and after magnification correction and used to train random forest (RF) models to classify high versus non-high myopia. Outcomes included classifier performance (the area under the receiver operating characteristic curve (AUC), sensitivity, specificity and feature importance) and changes in OCTA metrics between groups before and after correction.

Results: Image magnification correction significantly improved the classification of high versus non-high myopia. When all 14 features were used to train the model, the AUC increased from 0.77 (fair) to 0.88 (good), and when restricted to the top five features (fractal dimension (Df), vessel length density (VLD), branchpoint density (BD), parafoveal rim VLD, and vessel area density (VAD)), similarly, from 0.79 to 0.88.

Conclusions: OCTA image magnification correction improves RF classification of high myopia and clarifies inconsistencies across studies. Underreported metrics, fractal dimension, parafoveal rim VLD and BD, emerged as key discriminators. Magnification correction with ML may improve characterisation of myopia-related microvascular changes and enhance diagnostic precision, warranting further study.

Danuta M. Sampson and Mila Yue Zhang share co-first authorship.

This is an open access article under the terms of the Creative Commons Attribution-NonCommercial-NoDerivs License, which permits use and distribution in any medium, provided the original work is properly cited, the use is non-commercial and no modifications or adaptations are made.

© 2026 The Author(s). *Clinical & Experimental Ophthalmology* published by John Wiley & Sons Australia, Ltd on behalf of Royal Australian and New Zealand College of Ophthalmologists.

1 | Introduction

High myopia affects hundreds of millions of people worldwide and can cause irreversible vision loss due to progressive retinal and choroidal degeneration [1, 2]. As global prevalence continues to rise, especially among East Asian populations, there is a growing emphasis on developing effective diagnostic and treatment options [3, 4]. Given that high myopia can lead to progressive vision loss through degenerative and vascular alterations in the retina and choroid [5], understanding the relationship between pathological changes and perfusion is essential for improving disease detection and management. The blood flow monitoring techniques laser Doppler velocimetry and colour Doppler ultrasonography have been used in studies that have shown reduced retinal and choroidal blood flow in high myopia [6]. However, these techniques lack the resolution, depth discrimination and tissue contrast needed to accurately visualise the retinal microvasculature [6].

Optical coherence tomography angiography (OCTA) provides a non-invasive, high-resolution view of the retinal and choroidal microvasculature, enabling layer-specific assessment of microvascular characteristics, including commonly used metrics such as vessel area density (VAD) and vessel length density (VLD), as well as foveal avascular zone (FAZ) characteristics [7–9]. Collectively, these and other metrics, including fractal dimension (D_f), average of vessel diameter, average of vessel tortuosity (VT) and branchpoint density (BD), provide a comprehensive characterisation of retinal microvasculature. However, findings from OCTA studies in myopia remain inconsistent, with conflicting reports on VAD, VLD and foveal avascular zone area (FAZ-A) in superficial and deep vascular plexuses [10–38]. These discrepancies may stem from varying subject characteristics, myopia definitions (spherical equivalent (SE) vs. axial length (AL)), different sample sizes and whether OCTA image magnification error correction due to AL variations was applied [8, 39]. Despite strong evidence [40, 41] and international consensus recommending magnification error correction [42], 60% of the published studies reviewed for this article have not applied it, undermining the accuracy, comparability and clinical interpretability of reported microvascular metrics. In addition, while traditional statistical analyses applied in published papers have contributed to our understanding of retinal changes in high myopia, they may not fully capture the complex relationships between quantitative microvascular metrics and disease [43]. Machine learning (ML) methods can leverage high-dimensional data to identify subtle patterns that conventional approaches cannot detect, thereby supporting the generation of new knowledge and ultimately enhancing diagnostic and prognostic capabilities in clinical decision-making [43, 44]. ML research is a major driver of innovation and is already being rapidly adopted across ophthalmology [45]. In particular, the random forest (RF) model is attractive due to its capability to effectively capture intricate relationships within the input data and ability to tackle challenges associated with limited sample sizes without the risk of overfitting [43].

This study builds upon our previous publication in which we established the theoretical and empirical basis for OCTA image size correction based on AL assessment [40]. However, we did not assess how failing to apply this correction affects disease-classification model performance, as we now study herein. We hypothesise that correcting for image magnification error due to AL variations improves the accuracy and reliability of microvascular measurements and the downstream performance of classification models. Our primary aim is to assess improvement in classification accuracy when magnification error correction is implemented; the secondary aim is to examine how correction affects the values and discriminatory power of microvascular metrics, thereby seeking to address ongoing inconsistencies in the OCTA-myopia literature [5, 6]. Together, these analyses support the broader claim that image magnification error correction via AL assessment is not only a technical refinement but also a necessary preprocessing step for both the extraction of valid microvascular metrics and their use as features in robust ML models [42]. As ML models are increasingly applied to large, multi-site OCTA datasets, accurate and standardised input features become essential. Well-characterised OCTA-derived metrics help minimise bias and ensure reliable model performance, critical for advancing data-driven insights and improving patient outcomes in the era of open science and data sharing [8].

2 | Methods

2.1 | Study Participants

This study utilised retinal images from a prior study undertaken at the Optometry Research Clinic, School of Optometry, Hong Kong Polytechnic University, Hong Kong, China. Written informed consent, explaining the study procedures and potential risks, was obtained from all subjects. The study was approved by the University Ethics Committee (reference numbers HSEARS20170414001 and HSEARS20210122008). Subjects with any of the following conditions were excluded: systemic or ocular diseases that might affect ocular blood circulation; glaucomatous visual field defects; media opacities; history of ocular surgery or injury; best-corrected distance visual acuity measured in logarithm of minimum angle of resolution (logMAR) < 0.00; abnormal intraocular pressure > 21 mmHg; anisometropia (2.50 Dioptres [D] or above) and a history of smoking [46]. All subjects were asked to avoid alcohol and caffeine intake for 12 h before eye examination to minimise any disturbance to ocular circulation. A preliminary optometric examination was conducted to confirm the subject's eligibility and collect demographic data, including subjective refraction and best-corrected distance visual acuity. All participants underwent ophthalmic examination, including ocular biometry (IOL 500 Master; Carl Zeiss Meditec Inc., Jena, Germany) and autorefraction (Ryusyo Industrial Co. Ltd., Osaka, Japan). Subjects with extremely high myopia (spherical equivalent (SE) more myopic than −9.00 D) were additionally screened by static Humphrey Field Analyser (Carl Zeiss AG, Oberkochen, Germany) using the 24–2 fast Swedish Interactive Testing Algorithm to rule out visual field defects. A 3 × 3-mm macular OCTA scan was obtained with the Cirrus 5000 HD-OCT (Carl Zeiss AG, Oberkochen, Germany). The predefined standard AL for the Cirrus HD-OCT is 24.46 mm [47]. One eye from each subject was randomly selected and imaged. Image acquisition was conducted under natural pupil diameter, unless the area of interest was restricted by a small pupil size. In such cases, Mydrin-P (phenylephrine

14429071, 2026, 8, Downloaded from https://onlinelibrary.wiley.com/doi/10.1111/ceo.70162 by National Health And Medical Research Council, Wiley Online Library on [08/11/2026]. See the Terms and Conditions (https://onlinelibrary.wiley.com/terms-and-conditions) on Wiley Online Library for rules of use; OA articles are governed by the applicable Creative Commons License

hydrochloride 0.5% + tropicamide 0.5%; Santen Pharmaceutical Co. Ltd., Osaka, Japan) was used for dilation.

2.2 | OCTA Image Analysis

En-face OCTA images of the superficial vascular plexus (SVP) were obtained, and the Cirrus default SVP segmentation boundaries were applied. The instrument upper boundary is defined by the internal limiting membrane (ILM) and the lower boundary as ILM + 70% × the thickness between ILM and the outer plexiform layer (OPL) [47]. Images with motion artefacts, low signal strength, blur or poor centration were excluded using automated screening and visual inspection (DMS). Image analysis was performed using OCTAVA, an open-source tool developed by our group [47, 48]. Images were analysed twice: (1) assuming a nominal scan size of 3 × 3 mm (before correction) and (2) using Littman–Bennett-corrected scan dimensions (after correction) (Figure 1) [40, 49]. Before correction, all images were cropped to 2.8 × 2.8 mm and standardised to 1000 × 1000 pixels. After correction, images were first rescaled to their corrected dimensions, then cropped to 2.8 × 2.8 mm and standardised to 1000 × 1000 pixels. The 2.8-mm crop was chosen for all cases because it corresponded to the smallest corrected scan size in the dataset. All images were binarised using fuzzy means and a Frangi filter (kernel: 1–4 pixels). Skeletonisation applied an 8-pixel twig size. The FAZ was manually segmented from the uncorrected images, and the same contour was then applied to the corrected images.

Microvascular metrics were extracted from the full image area, the foveal circle (1.0-mm diameter circle that includes the FAZ) and the parafoveal rim (0.8-mm annulus around the foveal circle). No median filter was applied. The metrics extracted were: VAD, VLD, average of vessel diameter, BD, D_f, average of VT and the FAZ metrics: FAZ-area (FAZ-A); FAZ-perimeter (FAZ-P); FAZ-circularity (FAZ-C) and VAD around FAZ (FD-300, i.e., vessel density in a 300-μm diameter ring around the FAZ). D_f was calculated using a powers-of-2 box-size range (from 4 to 512 pixels). The definition of these metrics can be found elsewhere [8, 47]. Overall, 14 metrics were extracted and used as features in the RF classification task.

2.3 | Statistical Analysis

OCTA-derived metrics were statistically evaluated using IBM-SPSS (v26.0; IBM, Armonk, NY, USA), reporting mean and standard deviation (SD) over the subject group for each metric. Data distributions were assessed with the Shapiro–Wilk test. Paired *t*-tests compared corrected versus uncorrected images within groups, while unpaired *t*-tests compared metrics between groups. Statistical significance was initially defined as $p < 0.05$ (two-tailed). To account for multiple comparisons across the 14 OCTA-derived metrics, a Holm–Bonferroni correction was applied, resulting in an adjusted significance threshold. Both unadjusted and Holm–Bonferroni-adjusted *p*-values are reported where appropriate. Cohen's *d* was used to evaluate the effect size between groups [50–52].

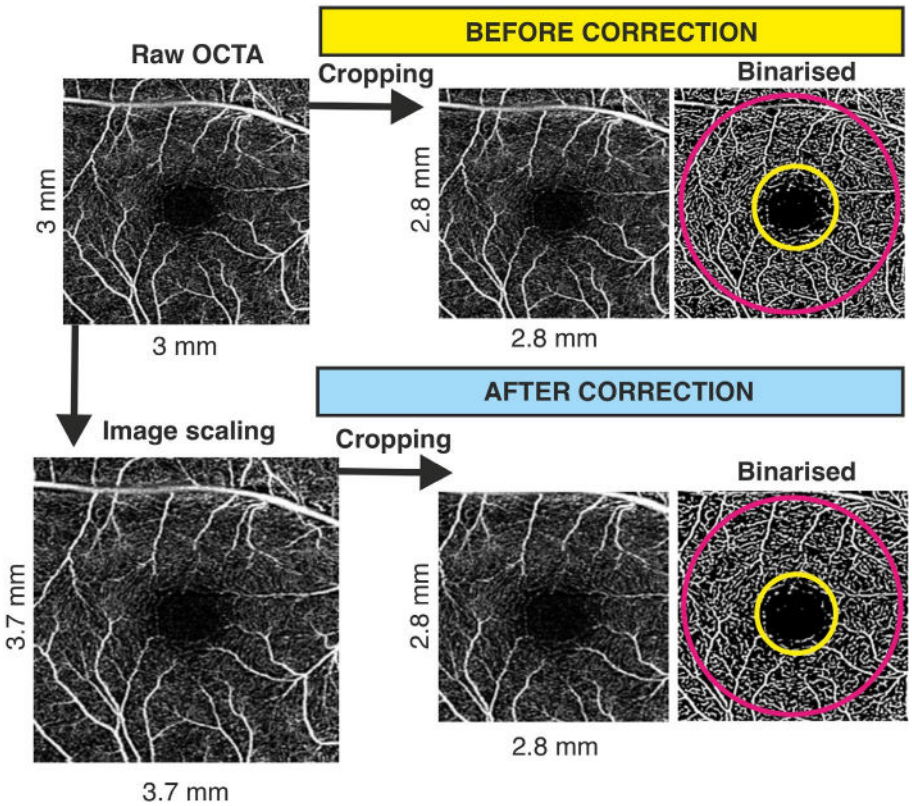


FIGURE 1 | Illustration of the image analysis workflow shows how OCTA image magnification error correction affects microvascular and FAZ metrics in a subject with a long AL (29.83 mm), exceeding the device's predefined standard axial length value of 24.46 mm. Before correction, the image is assumed to be 3 × 3 mm; after correction, the true size is 3.7 × 3.7 mm. The yellow circle and yellow/pink annulus define the foveal circle and parafoveal-rim, respectively.

14429071, 2026, 8, Downloaded from https://onlinelibrary.wiley.com/doi/10.1111/ceo.70162 by National Health And Medical Research Council, Wiley Online Library on [08/11/2026]. See the Terms and Conditions (https://onlinelibrary.wiley.com/terms-and-conditions) on Wiley Online Library for rules of use; OA articles are governed by the applicable Creative Commons License

We trained and tested RF models for classification tasks. Our methods are based on the approach described by Ahmed et al. [43], with the modification that we retained all microvascular and FAZ metrics as features in the initial RF model training and re-ranked feature (i.e., metric) importance, considering collinearity between the features based on the modified informative position (MIP) index [53]. The following conditions were studied: (i) non-high myopia versus high myopia (no magnification error correction) and (ii) non-high myopia versus high myopia (image magnification error correction applied). Stratified fivefold cross-validation was used to train and validate each RF model [54]. Out-of-fold (OOF) predictions for each trained model were aggregated to estimate uncertainty of classifier performance. RF classifier performance was reported with sensitivity, specificity and area under the receiver operating characteristic curve, abbreviated as area under the curve (AUC). AUC is widely used to evaluate classifier performance for binary classification tasks in which the classes are expected to be balanced [55]. The AUC is categorised as fail [0.50–0.60), poor [0.60–0.70), fair [0.70–0.80), good [0.80–0.90) or excellent [0.90–1.00] [56–59]. In the preceding, a square bracket indicates that the endpoint is included in the range, whereas a parenthesis indicates that the endpoint is excluded from the range. Generally, an AUC of at least 0.80 is considered acceptable [59]. Sensitivity and specificity are measures used to evaluate how well a screening/diagnostic method performs [60]. Sensitivity is the ability of a test to correctly identify people with the disease. Specificity is the ability of a test to correctly identify people who do not have the disease. In diagnostic accuracy studies, sensitivity and specificity values are often considered: unacceptable if less than 0.80, acceptable [0.80–0.89] or excellent [0.90–1.00] [60]. However, there is often a trade-off between sensitivity and specificity. In general, high sensitivity is more important for screening, whereas high specificity is more important for diagnosis [60].

OOF predictions were bootstrapped to compute 95% confidence intervals (95% CI) of the performance feature for each model and the change in AUC (ΔAUC) across bootstraps. The 95% CI of the ΔAUC was used to test the null hypotheses that models trained with and without AL correction are equivalent. The bootstrap *p*-value is evaluated using the distribution of ΔAUC as the reference distribution. Therefore, the *p*-value is equivalent to the fraction of bootstraps in which ΔAUC is less than zero [61]. An alpha value of 0.05 was used to evaluate statistical significance. Shapely Additive exPlanation (SHAP) values were calculated to describe the importance of each feature used for prediction in the RF classifier, generating a feature importance ranking [53]. SHAP assumes feature independence, however, many of the OCTA-derived metrics are not independent. Therefore, SHAP rankings were re-ordered using the MIP index, which further probes feature importance by iteratively removing the most important feature, retraining and summing importance across iterations [53, 62]. This ensures that OCTA features were ranked based on their contribution to the final prediction, regardless of collinearity between the metrics.

3 | Results

3.1 | Study Participants

One hundred and eighteen healthy young subjects aged between 18 and 40 years were recruited, including 51 with high myopia and 67 non-high myopes. Eight subjects were excluded from the analysis because of poor image quality, a decentred FAZ or an AL that, after correction, resulted in an image size of less than 2.8 mm. The non-high myopia group was defined as having a spherical equivalent less myopic than −6.00 D, while the high myopia group was defined as having a spherical equivalent equal to or more myopic than −6.00 D. The demographics and clinical characteristics of participants selected for this study are shown in Table 1.

3.2 | OCTA-Derived Quantitative Metrics

The SVP microvascular and FAZ metrics delivered by OCTAVA for OCTA images, uncorrected and corrected for magnification error, are summarised in Table 2. Significant differences in microvascular metrics were observed between study groups in both corrected and uncorrected OCTA images. Notably, the average of vessel diameter differed significantly between non-high and high myopia groups before correction but lost significance

TABLE 1 | Participant demographic data and summary of ocular biometry.

Parameters	Non-high myopia	High myopia
Number of participants	60	50
Number of eyes	60	50
Eyes (right:left)	32:28	27:23
Mean age (years) (standard deviation (SD), range)	25 (5, 18–40)	26 (6, 18–40)
Sex (male:female)	28:32	15:35
Mean axial length (mm) (SD, range)	24.72 (1.01, 22.94–27.51)	27.33 (1.45, 24.63–31.28)
Mean spherical equivalent (D) (SD, range)	−2.63 (1.91, −5.8 to +0.63)	−8.86 (2.23, −15.4 to −6.00)

14429071, 2026, 8, Downloaded from https://onlinelibrary.wiley.com/doi/10.1111/ceo.70162 by National Health And Medical Research Council, Wiley Online Library on [08/11/2026]. See the Terms and Conditions (https://onlinelibrary.wiley.com/terms-and-conditions) on Wiley Online Library for rules of use; OA articles are governed by the applicable Creative Commons License

TABLE 2 | Quantitative microvascular and foveal avascular zone metrics for images uncorrected and corrected for magnification error.

OCTA-derived metrics	Images uncorrected for axial length before assessment; values reported as mean (SD)					Images corrected for axial length before assessment; values reported as mean (SD)				
	NHM	HM	Dif.	*p-value*	*p**	NHM	HM	Dif.	*p*	*p**
VAD	36.4 (2.2)	33.9 (2.8)	−2.5	**<0.001**	**<0.001**	36.2 (2.4)	32.4 (3.4)	−3.8	**<0.001**	**<0.001**
VLD	21.2 (1.4)	19.7 (1.7)	−1.5	**<0.001**	**<0.001**	21.0 (1.7)	18.1 (2.0)	−2.9	**<0.001**	**<0.001**
Average of vessel diameter	17.9 (0.6)	17.2 (0.6)	−0.7	**<0.001**	**<0.001**	17.9 (0.5)	17.8 (0.6)	−0.1	0.362	0.724
BD	5.85 (0.77)	4.93 (0.73)	−0.93	**<0.001**	**<0.001**	5.82 (0.84)	4.56 (0.78)	−1.26	**<0.001**	**<0.001**
D_f	1.77 (0.01)	1.76 (0.02)	−0.01	**<0.001**	**<0.001**	1.77 (0.02)	1.74 (0.03)	−0.03	**<0.001**	**<0.001**
Average of VT	1.19 (0.01)	1.19 (0.01)	+0.00	0.056	0.281	1.19 (0.01)	1.19 (0.01)	+0.00	0.058	0.288
FAZ-A	0.25 (0.10)	0.22 (0.09)	−0.03	**0.047**	0.279	0.26 (0.10)	0.28 (0.12)	+0.02	0.376	0.376
FAZ-C	0.73 (0.13)	0.69 (0.16)	−0.04	0.246	0.99	0.73 (0.13)	0.69 (0.16)	−0.04	0.215	0.644
FAZ-P	2.06 (0.44)	2.01 (0.80)	−0.05	0.662	>0.99	2.08 (0.43)	2.28 (1.00)	+0.20	0.196	0.785
FD-300	36.5 (2.6)	33.8 (3.4)	−2.7	**<0.001**	**<0.001**	36.4 (2.8)	32.2 (4.0)	−4.2	**<0.001**	**<0.001**
Foveal circle VAD	19.4 (4.5)	19.6 (4.4)	+0.2	0.799	>0.99	19.0 (4.4)	16.1 (4.8)	−2.9	**0.001**	**0.003**
Foveal circle VLD	11.6 (2.6)	11.9 (2.7)	+0.3	0.575	>0.99	11.3 (2.6)	9.4 (2.9)	−1.9	**<0.001**	**<0.001**
Parafoveal rim VAD	37.5 (2.4)	34.7 (3.0)	−2.8	**<0.001**	**<0.001**	37.4 (2.6)	33.3 (3.6)	−4.1	**<0.001**	**<0.001**
Parafoveal rim VLD	22.0 (1.5)	20.3 (1.7)	−1.7	**<0.001**	**<0.001**	21.9 (1.7)	18.8 (2.1)	−3.1	**<0.001**	**<0.001**

Note: Highlighted in green, microvascular features where the between-group difference reversed direction and gained significance; orange, direction unchanged, significance lost; significant *p*-values (<0.05) are bolded.
Abbreviations: average of VT, average of vessel tortuosity [1]; BD, branchpoint density (nodes/mm); D_f, fractal dimension [1]; Dif., difference; FAZ-A, foveal avascular zone area (mm^2); FAZ-C, foveal avascular zone circularity (%); FAZ-P, foveal avascular zone perimeter (mm); FD-300, vessel density within 300-μm width rim surrounding the FAZ (%); foveal circle, parafoveal rim, unit of 1 indicates dimensionless; HM, high-myopia; NHM, non-high-myopia; *p*, unadjusted *p*-value; VAD, vessel area density (%); VLD, vessel length density (mm^{-1}), average of vessel diameter (μm).
*p, Holm–Bonferroni adjusted *p*-value.

after correction. The reversal trend occurred for FAZ-A, FAZ-P, foveal circle VAD and foveal circle VLD, though statistical significance varied by correction status.

Significant differences between uncorrected and corrected images were observed in most metrics within the high-myopia eyes (Table S1). There were no significant differences within the non-high-myopia study groups uncorrected versus corrected images. Generally, the effect size, measured by Cohen's *d*, between non-high and high myopic eyes was stronger after correction. Of note, corrected VLD, BD and parafoveal rim VLD showed the strongest effects with $d = 1.6$ (Table S2).

3.3 | Disease Classification

Applying image magnification error correction before feature extraction with OCTAVA significantly improved classification performance for non-high myopia versus high myopia. Using all 14 features, AUC increased from 0.77 (fair) to 0.88 (good) and using the top five features, from 0.79 (fair) to 0.88 (good) (Tables 3 and S3). Models with five features showed similar sensitivity and specificity to the model based on all 14 features (Table 3). BD, VLD, parafoveal rim VLD and VAD were consistently among the top 5 discriminative microvascular features for both classification tasks (Table 4). FAZ-related features did not significantly contribute to the classifier's performance.

4 | Discussion

In this cross-sectional study, we evaluated whether correcting AL-induced magnification errors in OCTA improves RF classification of high myopia and clarifies inconsistencies in the reported values and discriminatory power of OCTA-derived microvascular metrics. The non-parametric RF method does not rely on linear assumptions between features and is better suited to capturing nonlinear patterns and interactions among features. Previous studies have shown that RF improves automated disease classification in diabetic retinopathy, leading to better discrimination than traditional linear models [43].

14429071, 2026, 8, Downloaded from https://onlinelibrary.wiley.com/doi/10.1111/ceo.70162 by National Health And Medical Research Council, Wiley Online Library on [08/11/2026]. See the Terms and Conditions (https://onlinelibrary.wiley.com/terms-and-conditions) on Wiley Online Library for rules of use; OA articles are governed by the applicable Creative Commons License

TABLE 3 | Mean area under the receiver operating characteristic curve (AUC) for tested classification tasks.

Classification task	Image scaling	AUC	Sensitivity	Specificity
Based on all 14 features				
Non-high myopia versus high myopia	Uncorrected	0.77 (0.75–0.79)	0.68 (0.65–0.71)	0.72 (0.70–0.75)
	Corrected	0.88 (0.87–0.90)	0.77 (0.75–0.80)	0.82 (0.80–0.85)
		Mean ΔAUC: 0.14 (0.08–0.20), $p < 0.001$		
Based on top 5 features in each model				
Non-high myopia versus high myopia	Uncorrected	0.79 (0.77–0.81)	0.68 (0.66–0.71)	0.72 (0.70–0.75)
	Corrected	0.88 (0.87–0.89)	0.79 (0.76–0.81)	0.84 (0.82–0.86)
		Mean ΔAUC: 0.11 (0.06–0.17), $p < 0.001$		

Note: AUC can be categorised as fail [0.5–0.6), poor [0.6–0.7), fair [0.70–0.80), good [0.80–0.90) or excellent [0.90–1.0]. In diagnostic accuracy studies, sensitivity and specificity values are often considered: unacceptable if less than 0.80, acceptable [0.80–0.89] or excellent [0.90–1.00] [60]. ΔAUC, the change in AUC between models.

TABLE 4 | Feature importance ranking: features were derived from SVP OCTA images prior to (left) or after (right) magnification error correction and used as inputs to train an RF classification algorithm for the task listed.

	Uncorrected OCTA images		Corrected OCTA images	
	Feature	Ranking[a]	Feature	Ranking
Non-high myopia versus high myopia	Average of vessel diameter (μm)	1	Fractal dimension [1]	1
	BD (nodes/mm)	2	VLD (mm^{-1})	2
	VLD (mm^{-1})	3	BD (nodes/mm)	3
	Parafoveal rim VLD (mm^{-1})	4	Parafoveal rim VLD (mm^{-1})	4
	VAD (%)	5	VAD (%)	5

Note: A consistent colour scheme is employed to denote identical features in both groups to enhance data visibility and comparability.
Abbreviations: BD, branchpoint density; VAD, vessel area density; VLD, vessel length density.
[a]Ranking based on methods described in [53].

We showed that correcting for image magnification error between non–high- and high-myopia groups significantly improved RF classification performance. A model incorporating five key features achieved similar sensitivity and specificity, suggesting that these features efficiently capture the relationship between non-high-myopia and high-myopia groups while reducing computational time [63, 64]. Consistent with this, Cohen's *d* values (Table S2) indicated that the five selected features (Table 4) exhibited the largest effect sizes (≥1.3), suggesting that effect-size measures can effectively guide feature prioritisation for RF-based classification.

The RF model identified fractal dimension (D_f), VLD, BD, parafoveal rim VLD and VAD as the five most influential features for high-myopia classification. Notably, D_f, BD and parafoveal VLD are relatively underreported in the literature; however, their prominence in the model suggests that, after correction for axial length, they may capture microvascular alterations not fully characterised to date. These findings indicate that further investigation of these features in large cohorts may provide additional insight into microvascular changes across different stages of myopia. This is particularly important because, despite numerous studies investigating myopia-related vascular changes, it remains unclear whether and how the ocular blood supply is affected by myopia-induced eyeball elongation, given the contradictory evidence [5].

In this study, we showed that applying the correction altered intergroup differences in OCTA metrics, helping to clarify inconsistencies reported in prior studies. Such differences are expected, as the true size of the fundus image is dependent on the combined magnification of the imaging device and the eye [39]. Commercial OCTA instruments provide retinal scan areas in mm^2 units. The lateral scale is obtained by calculating the curvilinear distance on the surface subtended by the fixed angular field of view using a 'standard' AL predefined independently by each instrument maker. Since the AL is predefined, it does not account for the differences in AL between subjects [40, 41, 65]. To ensure accurate quantitative analysis, images should be corrected for lateral magnification based on the actual AL of each eye. That said, image magnification error correction is not required for longitudinal monitoring of individuals [65] or for other instances in which no significant change in AL is expected. It is also worth noting that some OCTA-derived metrics are not impacted by AL, including FAZ-C and D_f [66]. Despite growing awareness, 60% of studies published after 2023 and reviewed for this article did not apply magnification error correction, raising concerns about the accuracy, comparability and contribution to conflicting findings in the literature. Some studies report reduced SVP VAD [10–24], VLD [16, 19, 25, 26] and enlarged FAZ-A [15, 27–31], while others find no significant differences compared to emmetropes or low myopes [26, 32–37]. Discrepancies between

14429071, 2026, 8, Downloaded from https://onlinelibrary.wiley.com/doi/10.1111/ceo.70162 by National Health And Medical Research Council, Wiley Online Library on [08/11/2026]. See the Terms and Conditions (https://onlinelibrary.wiley.com/terms-and-conditions) on Wiley Online Library for rules of use; OA articles are governed by the applicable Creative Commons License

studies of the deep capillary plexus (DCP) are also found in the literature [11–13, 16, 33, 34, 38].

Our study found that high myopes exhibited significantly lower SVP VAD, VLD, BD and D_f, regardless of correction. VAD, VLD, BD, D_f, parafoveal rim VAD and parafoveal rim VLD showed increased discriminatory power after correction (Table S2). Our observed VAD and D_f reductions in high myopes were also previously reported in OCTA studies [24, 37].

Regarding foveal circle VAD, Meng et al., who did not apply correction, found no differences between groups, aligning with our statistically insignificant uncorrected results [20]. However, after correction, we observed statistically significant foveal circle VAD changes. The mean difference in FAZ-A and FAZ-P (high myopes versus non-high myopes) shifted from negative to positive. FAZ-A differences were significant before correction, but were no longer significant after Holm-Bonferroni adjustment or AL correction, consistent with prior studies that applied and reported correction [15, 27–29, 31]. This finding also aligns with the broader literature, which indicates that FAZ size and shape can vary considerably across individuals [67, 68]. Ours and others' observed altered direction, magnitude and significance of OCTA-derived metrics due to magnification error correction strongly indicate that uncorrected comparisons are biased and misleading. Reversals in the direction of effect suggest that some previously reported microvascular changes may reflect imaging artefacts rather than true physiological differences.

The SVP average of vessel diameter for high myopes versus non-high myopes decreased in magnitude and lost significance after correction. This finding is consistent with a previous study using fundus photography, which reported a decrease or no change in vessel diameter with increasing myopia in average retinal arteriolar (~110 μm) and venular vessel diameter (~165 μm) [69]. Fundus photography-based studies reporting a significant decrease did not account for ocular magnification; therefore, the reported association may have been attributable to this omission [70, 71]. Yii et al. [72], Cheung et al. [73] and Wong et al. [69] all reported that the significant negative association between vessel diameter and myopia disappeared after correction for magnification error. Wong et al. showed that the correction had minimal effect on vessel diameter in emmetropic eyes (193.2–192.5 μm) but altered measurements in high myopia (162.5–190.1 μm), findings that align with our study.

Our study has several important limitations. First, it is a small cross-sectional design; a longitudinal, large-cohort design would provide a better understanding of how microvascular changes evolve with increasing myopia and high myopia. Eyes with advanced myopic pathology, such as severe myopic degeneration or macular complications, were not included due to limited cohort size and the fact that many highly myopic patients with advanced changes had already undergone treatment. We also did not evaluate the DCP, even though it may play a role in microvascular alterations associated with myopic progression. The imaging field was restricted to the macular region, excluding the assessment of peripheral retinal changes. Finally, because the Littmann-Bennett correction incorporates each participant's AL, the resulting OCTA metrics are partially dependent on AL. Given the strong association between AL and high myopia, some of the predictive performance may reflect AL-related scaling effects rather than exclusively capturing disease-specific microvascular alterations. Future studies should consider additional analyses that control for AL or include AL as a separate covariate. This would help clarify the extent to which model performance is driven by disease-specific microvascular features rather than AL-related information that may be implicity embedded in OCTA features following magnification correction.

4.1 | Conclusions

In this cross-sectional study, we show that using individual AL to correct for image magnification error significantly improves classification between non-high and high myopia based on a RF ML model. Features such as fractal dimension (D_f), BD, parafoveal rim VLD, infrequently reported in the literature, emerged among the top five discriminators, highlighting the potential of ML to reveal unexpected new informative microvascular changes. Additionally, magnification error correction altered the direction of change, strength, and/or statistical significance of some OCTA-derived metrics, underscoring its importance in accurately assessing retinal microvascular changes across myopia stages. With the growing use of large, multi-site OCTA datasets for classification tasks and evidence presented here and elsewhere that magnification error correction can improve the accuracy of microvascular features and can maintain or enhance model performance, we recommend applying image magnification error correction in OCTA-based analyses, as well as applying ML for probing the nonlinear relationships between microvascular features. If correction is not feasible, it should be clearly stated as a study limitation.

Acknowledgements

This activity has been supported by the Western Australian Future Health Research and Innovation Fund (grant ID IF2024-25/5; D.M.S.). Open access publishing facilitated by The University of Western Australia, as part of the Wiley - The University of Western Australia agreement via the Council of Australasian University Librarians.

Funding

This work was supported by the Department of Health, Government of Western Australia (IF2024-25/5).

Conflicts of Interest

The authors declare no conflicts of interest.

Data Availability Statement

The data that support the findings of this study are available on request from the corresponding author. The data are not publicly available due to privacy or ethical restrictions.

References

1. P. N. Baird, S. M. Saw, C. Lanca, et al., "Myopia," *Nature Reviews Disease Primers* 6, no. 1 (2020): 99.

2. D. I. Flitcroft, M. He, J. B. Jonas, et al., "IMI—Defining and Classifying Myopia: A Proposed Set of Standards for Clinical and Epidemiologic

14429071, 2026, 8, Downloaded from https://onlinelibrary.wiley.com/doi/10.1111/ceo.70162 by National Health And Medical Research Council, Wiley Online Library on [08/11/2026]. See the Terms and Conditions (https://onlinelibrary.wiley.com/terms-and-conditions) on Wiley Online Library for rules of use; OA articles are governed by the applicable Creative Commons License

Studies," *Investigative Ophthalmology & Visual Science* 60, no. 3 (2019): M20–M30.

3. B. A. Holden, T. R. Fricke, D. A. Wilson, et al., "Global Prevalence of Myopia and High Myopia and Temporal Trends From 2000 Through 2050," *Ophthalmology* 123, no. 5 (2016): 1036–1042.

4. W. Pan, S.-M. Saw, T. Y. Wong, I. Morgan, Z. Yang, and W. Lan, "Prevalence and Temporal Trends in Myopia and High Myopia Children in China: A Systematic Review and Meta-Analysis With Projections From 2020 to 2050," *Lancet Regional Health - Western Pacific* 55 (2025): 101484.

5. M. Zhao, A. K. Lam, and A. M. Cheong, "Structural and Haemodynamic Properties of Ocular Vasculature in Axial Myopia," *Clinical and Experimental Optometry* 105, no. 3 (2022): 247–262.

6. Z. X. Lin, F. Tang, X. J. Zhang, et al., "Retinal and Choroidal Microvasculature at Different Myopia Severities: A Systematic Review and Meta-Analysis," *Ophthalmology Science* 6, no. 1 (2026): 100921.

7. R. F. Spaide, J. G. Fujimoto, N. K. Waheed, S. R. Sadda, and G. Staurenghi, "Optical Coherence Tomography Angiography," *Progress in Retinal and Eye Research* 64 (2018): 1–55.

8. D. M. Sampson, A. M. Dubis, F. K. Chen, R. J. Zawadzki, and D. D. Sampson, "Towards Standardizing Retinal Optical Coherence Tomography Angiography: A Review," *Light: Science & Applications* 11, no. 1 (2022): 63.

9. T. T. Hormel, Y. Jia, Y. Jian, et al., "Plexus-Specific Retinal Vascular Anatomy and Pathologies as Seen by Projection-Resolved Optical Coherence Tomographic Angiography," *Progress in Retinal and Eye Research* 80 (2021): 100878.

10. M. Al-Sheikh, N. Phasukkijwatana, R. Dolz-Marco, et al., "Quantitative OCT Angiography of the Retinal Microvasculature and the Choriocapillaris in Myopic Eyes," *Investigative Ophthalmology & Visual Science* 58, no. 4 (2017): 2063–2069.

11. H. Fan, H. Y. Chen, H. J. Ma, et al., "Reduced Macular Vascular Density in Myopic Eyes," *Chinese Medical Journal* 130, no. 4 (2017): 445–451.

12. J. Mo, A. Duan, S. Chan, X. Wang, and W. Wei, "Vascular Flow Density in Pathological Myopia: An Optical Coherence Tomography Angiography Study," *BMJ Open* 7, no. 2 (2017): e013571.

13. W. Elsherif, M. Moustafa, H. Attaallah, and R. Hassanien, "Macular Microvaculature Evaluation Using Optical Coherence Tomography Angiography in Patients With High Myopia," *Egyptian Retina Journal* 6, no. 2 (2019): 43–51.

14. D. W. Yang, D. Cao, L. Zhang, et al., "Macular and Peripapillary Vessel Density in Myopic Eyes of Young Chinese Adults," *Clinical & Experimental Optometry* 103, no. 6 (2020): 830–837.

15. C. H. Min, H. M. Al-Qattan, J. Y. Lee, J. G. Kim, Y. H. Yoon, and Y. J. Kim, "Macular Microvasculature in High Myopia Without Pathologic Changes: An Optical Coherence Tomography Angiography Study," *Korean Journal of Ophthalmology* 34, no. 2 (2020): 106–112.

16. L. Su, Y.-S. Ji, N. Tong, et al., "Quantitative Assessment of the Retinal Microvasculature and Choriocapillaris in Myopic Patients Using Swept-Source Optical Coherence Tomography Angiography," *Graefe's Archive for Clinical and Experimental Ophthalmology* 258 (2020): 1173–1180.

17. T. Ucak, E. Icel, H. Yilmaz, et al., "Alterations in Optical Coherence Tomography Angiography Findings in Patients With High Myopia," *Eye* 34, no. 6 (2020): 1129–1135.

18. J. Gu, Y. Xu, D. Xiao, et al., "Peripheral Superficial Retina Vascular Density and Area of Radial Peripapillary Capillaries Changes in Myopic Individuals: A Wide-Field OCT Angiography Study," *Translational Vision Science & Technology* 13, no. 9 (2024): 21.

19. M. L. J. Živković, L. Lazić, M. Zlatanovic, et al., "The Influence of Myopia on the Foveal Avascular Zone and Density of Blood Vessels of the Macula—An OCTA Study," *Medicina (Kaunas, Lithuania)* 59, no. 3 (2023): 452.

20. Y. Meng, Z. H. Yi, Y. S. Xu, L. He, L. Li, and C. Z. Chen, "Changes in Macular Vascular Density and Retinal Thickness in Young Myopic Adults Without Pathological Changes: An OCTA Study," *European Review for Medical and Pharmacological Sciences* 26, no. 16 (2022): 5736–5744.

21. T. Wang, H. Li, R. Zhang, Y. Yu, X. Xiao, and C. Wu, "Evaluation of Retinal Vascular Density and Related Factors in Youth Myopia Without Maculopathy Using OCTA," *Scientific Reports* 11, no. 1 (2021): 15361.

22. M. Liu, P. Wang, X. Hu, C. Zhu, Y. Yuan, and B. Ke, "Myopia-Related Stepwise and Quadrant Retinal Microvascular Alteration and Its Correlation With Axial Length," *Eye* 35, no. 8 (2021): 2196–2205.

23. J. Gołębiewska, K. Biała-Gosek, A. Czeszyk, and W. Hautz, "Optical Coherence Tomography Angiography of Superficial Retinal Vessel Density and Foveal Avascular Zone in Myopic Children," *PLoS One* 14, no. 7 (2019): e0219785.

24. Y. Yang, J. Wang, H. Jiang, et al., "Retinal Microvasculature Alteration in High Myopia," *Investigative Ophthalmology & Visual Science* 57, no. 14 (2016): 6020–6030.

25. X. Zhu, J. Meng, L. Wei, K. Zhang, W. He, and Y. Lu, "Cilioretinal Arteries and Macular Vasculature in Highly Myopic Eyes: An Oct Angiography-Based Study," *Ophthalmology Retina* 4, no. 10 (2020): 965–972.

26. L. Lin, X. Zhang, C. Huang, and Z. Zhang, "Evaluation of Retinal Vascular Density and Related Factors Using OCTA in Children and Adolescents With Myopia Without Maculopathy," *Journal of International Medical Research* 51, no. 1 (2023): 3000605221150136.

27. M. S. Sung, T. H. Lee, H. Heo, and S. W. Park, "Association Between Optic Nerve Head Deformation and Retinal Microvasculature in High Myopia," *American Journal of Ophthalmology* 188 (2018): 81–90.

28. J. He, Q. Chen, Y. Yin, et al., "Association Between Retinal Microvasculature and Optic Disc Alterations in High Myopia," *Eye* 33 (2019): 1494–1503.

29. H. Piao, Y. Guo, H. Zhang, M. S. Sung, and S. W. Park, "Acircularity and Circularity Indexes of the Foveal Avascular Zone in High Myopia," *Scientific Reports* 11, no. 1 (2021): 16808.

30. J. H. Lee, M. W. Lee, S. K. Baek, and Y. H. Lee, "Repeatability of Manual Measurement of Foveal Avascular Zone Area in Optical Coherence Tomography Angiography Images in High Myopia," *Korean Journal of Ophthalmology* 34, no. 2 (2020): 113–120.

31. S. W. Wang, K. C. Hung, C. Y. Tsai, M. S. Chen, and T. C. Ho, "Myopic Traction Maculopathy Biomarkers on Optical Coherence Tomography Angiography—An Overlooked Mechanism of Visual Acuity Correction in Myopic Eyes," *Eye* 33, no. 8 (2019): 1305–1313.

32. X. Wang, X. Kong, C. Jiang, M. Li, J. Yu, and X. Sun, "Is the Peripapillary Retinal Perfusion Related to Myopia in Healthy Eyes? A Prospective Comparative Study," *BMJ Open* 6, no. 3 (2016): e010791.

33. S. Q. Yang, M. W. Zhou, B. Lu, et al., "Quantification of Macular Vascular Density Using Optical Coherence Tomography Angiography and Its Relationship With Retinal Thickness in Myopic Eyes of Young Adults," *Journal of Ophthalmology* 2017 (2017): 1–10.

34. R. Venkatesh, S. Sinha, D. Gangadharaiah, et al., "Retinal Structural–Vascular–Functional Relationship Using Optical Coherence Tomography and Optical Coherence Tomography—Angiography in Myopia," *Eye and Vision* 6, no. 1 (2019): 8.

35. Y. Guo, M. S. Sung, and S. W. Park, "Assessment of Superficial Retinal Microvascular Density in Healthy Myopia," *International Ophthalmology* 39, no. 8 (2019): 1861–1870.

36. F. Xiong, T. Mao, J. Wang, J. Yi, Y. Hu, and H. Liao, "Superficial Retinal Vessel Density and Foveal Avascular Zone in Myopic Anisometropia:

14429071, 2026, 8, Downloaded from https://onlinelibrary.wiley.com/doi/10.1111/ceo.70162 by National Health And Medical Research Council, Wiley Online Library on [08/11/2026]. See the Terms and Conditions (https://onlinelibrary.wiley.com/terms-and-conditions) on Wiley Online Library for rules of use; OA articles are governed by the applicable Creative Commons License

An OCTA-Based Study in Young Chinese Children," *BioMed Research International* 2022, no. 1 (2022): 1229009.

37. M. Li, Y. Yang, H. Jiang, et al., "Retinal Microvascular Network and Microcirculation Assessments in High Myopia," *American Journal of Ophthalmology* 174 (2017): 56–67.

38. Q. Zhu, X. Xing, M. Wang, et al., "Characterization of the Three Distinct Retinal Capillary Plexuses Using Optical Coherence Tomography Angiography in Myopic Eyes," *Translational Vision Science & Technology* 9, no. 4 (2020): 8.

39. D. F. Garway-Heath, A. R. Rudnicka, T. Lowe, P. J. Foster, F. W. Fitzke, and R. A. Hitchings, "Measurement of Optic Disc Size: Equivalence of Methods to Correct for Ocular Magnification," *British Journal of Ophthalmology* 82, no. 6 (1998): 643–649.

40. D. M. Sampson, P. Gong, D. An, et al., "Axial Length Variation Impacts on Superficial Retinal Vessel Density and Foveal Avascular Zone Area Measurements Using Optical Coherence Tomography Angiography," *Investigative Ophthalmology & Visual Science* 58, no. 7 (2017): 3065–3072.

41. S. Llanas, R. E. Linderman, F. K. Chen, and J. Carroll, "Assessing the Use of Incorrectly Scaled Optical Coherence Tomography Angiography Images in Peer-Reviewed Studies: A Systematic Review," *JAMA Ophthalmology* 138, no. 1 (2020): 86–94.

42. M. R. Munk, A. H. Kashani, R. Tadayoni, et al., "Recommendations for OCT Angiography Reporting in Retinal Vascular Disease: A Delphi Approach by International Experts," *Ophthalmology Retina* 6, no. 9 (2022): 753–761.

43. T. S. Ahmed, J. Shah, Y. N. B. Zhen, et al., "Ocular Microvascular Complications in Diabetic Retinopathy: Insights From Machine Learning," *BMJ Open Diabetes Research & Care* 12, no. 1 (2024): e003758.

44. L. Adlung, Y. Cohen, U. Mor, and E. Elinav, "Machine Learning in Clinical Decision Making," *Medicus* 2, no. 6 (2021): 642–665.

45. P. Yang and B. Yang, "Development and Validation of Predictive Models for Diabetic Retinopathy Using Machine Learning," *PLoS One* 20, no. 2 (2025): e0318226.

46. M. Zhao, A. K. Lam, M. T. Ying, and A. M. Cheong, "Hemodynamic and Morphological Changes of the Central Retinal Artery in Myopic Eyes," *Scientific Reports* 12, no. 1 (2022): 7104.

47. G. R. Untracht, M. S. Durkee, M. Zhao, et al., "Towards Standardising Retinal OCT Angiography Image Analysis With Open-Source Toolbox OCTAVA," *Scientific Reports* 14, no. 1 (2024): 5979.

48. G. R. Untracht, R. S. Matos, N. Dikaios, et al., "OCTAVA: An Open-Source Toolbox for Quantitative Analysis of Optical Coherence Tomography Angiography Images," *PLoS One* 16, no. 12 (2021): e0261052.

49. A. G. Bennett, A. R. Rudnicka, and D. F. Edgar, "Improvements on Littmann's Method of Determining the Size of Retinal Features by Fundus Photography," *Graefe's Archive for Clinical and Experimental Ophthalmology* 232, no. 6 (1994): 361–367.

50. G. M. Sullivan and R. Feinn, "Using Effect Size-Or Why the p Value Is Not Enough," *Journal of Graduate Medical Education* 4, no. 3 (2012): 279–282.

51. D. K. Lee, "Alternatives to p Value: Confidence Interval and Effect Size," *Korean Journal of Anesthesiology* 69, no. 6 (2016): 555–562.

52. D. Lakens, "Calculating and Reporting Effect Sizes to Facilitate Cumulative Science: A Practical Primer for t-Tests and ANOVAs," *Frontiers in Psychology* 4 (2013): 863.

53. A. M. Salih, Z. Raisi-Estabragh, I. B. Galazzo, et al., "A Perspective on Explainable Artificial Intelligence Methods: SHAP and LIME," *Advanced Intelligent Systems* 7, no. 1 (2025): 2400304.

54. T. Fontanari, T. C. Fróes, and M. Recamonde-Mendoza, "Cross-Validation Strategies for Balanced and Imbalanced Datasets," in *Intelligent Systems: 11th Brazilian Conference, BRACIS 2022, Proceedings, Part I* (Springer-Verlag, 2022), 626–640.

55. C. E. Metz, "Basic Principles of ROC Analysis," *Seminars in Nuclear Medicine* 8, no. 4 (1978): 283–298.

56. F. Li and H. He, "Assessing the Accuracy of Diagnostic Tests," *Shanghai Archives of Psychiatry* 30, no. 3 (2018): 207–212.

57. S. A. Hicks, I. Strümke, V. Thambawita, et al., "On Evaluation Metrics for Medical Applications of Artificial Intelligence," *Scientific Reports* 12, no. 1 (2022): 5979.

58. Ş. K. Çorbacıoğlu and G. Aksel, "Receiver Operating Characteristic Curve Analysis in Diagnostic Accuracy Studies: A Guide to Interpreting the Area Under the Curve Value," *Turkish Journal of Emergency Medicine* 23, no. 4 (2023): 195–198.

59. F. S. Nahm, "Receiver Operating Characteristic Curve: Overview and Practical Use for Clinicians," *Korean Journal of Anesthesiology* 75, no. 1 (2022): 25–36.

60. A. Walshe, E. Daly, and L. Ryan, "Clinical Utility of Ocular Assessments in Sport-Related Concussion: A Scoping Review," *Journal of Functional Morphology and Kinesiology* 9, no. 3 (2024): 157.

61. H. Qiyuan, M. W. Heather, and L. G. Maryellen, "Radiomics Methodology for Breast Cancer Diagnosis Using Multiparametric Magnetic Resonance Imaging," *Journal of Medical Imaging* 7, no. 4 (2020): 044502.

62. A. M. Salih, I. B. Galazzo, Z. Raisi-Estabragh, S. E. Petersen, G. Menegaz, and P. Radeva, "Characterizing the Contribution of Dependent Features in XAI Methods," *IEEE Journal of Biomedical and Health Informatics* 28, no. 11 (2024): 6466–6473.

63. G. Chandrashekar and F. Sahin, "A Survey on Feature Selection Methods," *Computers and Electrical Engineering* 40, no. 1 (2014): 16–28.

64. K.-C. Lin, J. C. Hung, and J.-t. Wei, "Feature Selection With Modified Lion's Algorithms and Support Vector Machine for High-Dimensional Data," *Applied Soft Computing* 68 (2018): 669–676.

65. F. K. Chen, M. Menghini, A. Hansen, D. A. Mackey, I. J. Constable, and D. M. Sampson, "Intrasession Repeatability and Interocular Symmetry of Foveal Avascular Zone and Retinal Vessel Density in OCT Angiography," *Translational Vision Science & Technology* 7, no. 1 (2018): 6.

66. B. D. Krawitz, S. Mo, L. S. Geyman, et al., "Acircularity Index and Axis Ratio of the Foveal Avascular Zone in Diabetic Eyes and Healthy Controls Measured by Optical Coherence Tomography Angiography," *Vision Research* 139 (2017): 177–186.

67. A. M. Dubis, B. R. Hansen, R. F. Cooper, J. Beringer, A. Dubra, and J. Carroll, "Relationship Between the Foveal Avascular Zone and Foveal Pit Morphology," *Investigative Ophthalmology & Visual Science* 53, no. 3 (2012): 1628–1636.

68. J. Chua, B. Tan, D. Wong, et al., "Optical Coherence Tomography Angiography of the Retina and Choroid in Systemic Diseases," *Progress in Retinal and Eye Research* 103 (2024): 101292.

69. T. Y. Wong, J. J. Wang, E. Rochtchina, R. Klein, and P. Mitchell, "Does Refractive Error Influence the Association of Blood Pressure and Retinal Vessel Diameters? The Blue Mountains Eye Study," *American Journal of Ophthalmology* 137, no. 6 (2004): 1050–1055.

70. T. Y. Wong, M. D. Knudtson, R. Klein, B. E. Klein, S. M. Meuer, and L. D. Hubbard, "Computer-Assisted Measurement of Retinal Vessel Diameters in the Beaver Dam Eye Study: Methodology, Correlation Between Eyes, and Effect of Refractive Errors," *Ophthalmology* 111, no. 6 (2004): 1183–1190.

71. N. Patton, R. Maini, T. MacGillivary, T. M. Aslam, I. J. Deary, and B. Dhillon, "Effect of Axial Length on Retinal Vascular Network Geometry," *American Journal of Ophthalmology* 140, no. 4 (2005): 648–653.

72. F. Yii, N. Strang, C. Moulson, B. Dhillon, M. O. Bernabeu, and T. MacGillivray, "The Optical Nature of Myopic Changes in Retinal Vessel Caliber," *Ophthalmology Science* 5, no. 1 (2025): 100631.

14429071, 2026, 8, Downloaded from https://onlinelibrary.wiley.com/doi/10.1111/ceo.70162 by National Health And Medical Research Council, Wiley Online Library on [08/11/2026]. See the Terms and Conditions (https://onlinelibrary.wiley.com/terms-and-conditions) on Wiley Online Library for rules of use; OA articles are governed by the applicable Creative Commons License

73. N. Cheung, G. Tikellis, S. M. Saw, et al., "Relationship of Axial Length and Retinal Vascular Caliber in Children," *American Journal of Ophthalmology* 144, no. 5 (2007): 658–662.

Supporting Information

Additional supporting information can be found online in the Supporting Information section. **Table S1:** Difference of means (Dif.) within study groups for images corrected versus uncorrected for magnification error, for each OCTA feature based on the superficial vascular plexus (SVP) and a paired *t* test. **Table S2:** Effect size reported by Cohen's *d* correction and 95% confidence intervals for each microvascular and foveal avascular zone metric in the SVP between study groups for images pre- and post-correction for magnification. **Table S3:** Random forest model hyperparameter tuning.

14429071, 2026, 8, Downloaded from https://onlinelibrary.wiley.com/doi/10.1111/ceo.70162 by National Health And Medical Research Council, Wiley Online Library on [08/11/2026]. See the Terms and Conditions (https://onlinelibrary.wiley.com/terms-and-conditions) on Wiley Online Library for rules of use; OA articles are governed by the applicable Creative Commons License